Topology optimization for worst load conditions based on the eigenvalue analysis of an aggregated linear system

Akihiro Takezawa[a,*], Satoru Nii[b], Mitsuru Kitamura[a], Nozomu Kogiso[c]

[a] *Division of Mechanical Systems and Applied Mechanics, Faculty of Engineering, Hiroshima University, 1-4-1 Kagamiyama, Higashi-Hiroshima, Hiroshima, Japan*
[b] *Department of Transportation and Environmental Systems, Graduate School of Engineering, Hiroshima University, 1-4-1 Kagamiyama, Higashi-Hiroshima, Hiroshima, Japan*
[c] *Department of Aerospace Engineering, Graduate School of Engineering, Osaka Prefecture University, 1-1 Gakuen-Cho, Naka-Ku, Sakai, Osaka, Japan*

Abstract

This paper proposes a topology optimization for a linear elasticity design problem subjected to an uncertain load. The design problem is formulated to minimize a robust compliance that is defined as the maximum compliance induced by the worst load case of an uncertain load set. Since the robust compliance can be formulated as the scalar product of the uncertain input load and output displacement vectors, the idea of "aggregation" used in the field of control is introduced to assess the value of the robust compliance. The aggregation solution technique provides the direct relationship between the uncertain input load and output displacement, as a small linear system composed of these vectors and the reduced size of a symmetric matrix, in the context of a discretized linear elasticity problem, using the finite element

*Corresponding author. Tel:+81-82-424-7544; Fax:+81-82-422-7194
Email addresses: akihiro@hiroshima-u.ac.jp (Akihiro Takezawa), m094172@hiroshima-u.ac.jp (Satoru Nii), kitamura@naoe.hiroshima-u.ac.jp (Mitsuru Kitamura), kogiso@aero.osakafu-u.ac.jp (Nozomu Kogiso)

Preprint submitted to Computer Methods in Applied Mechanics and Engineering May 12, 2011

method. Introducing the constraint that the Euclidean norm of the uncertain load set is fixed, the robust compliance minimization problem is formulated as the minimization of the maximum eigenvalue of the aggregated symmetric matrix according to the Rayleigh-Ritz theorem for symmetric matrices. Moreover, the worst load case is easily established as the eigenvector corresponding to the maximum eigenvalue of the matrix. The proposed structural optimization method is implemented using topology optimization and the method of moving asymptotes (MMA). The numerical examples provided illustrate mechanically reasonable structures and establish the worst load cases corresponding to these optimal structures.
Keywords: Robust design, Worst case design, Topology optimization, Finite element method, Eigenvalue analysis, Sensitivity analysis

1. Introduction

The search for optimal structural shapes under various conditions is a very important, challenging and attractive subject for researchers and engineers. Research on structural optimization has a history spanning more than a century in both mechanical and mathematical fields, and can be found in textbooks such as [1, 2, 3, 4, 5, 6, 7]. In particular, topology optimization has been extensively applied to a variety of structural optimization problems [6] since Bendsøe and Kikuchi first proposed a so-called homogenization design method (HDM) [8]. This method offers the greatest potential for exploring ideal and optimized structures because it allows changes in topology as well as shape.

Although the physical properties, mechanical conditions and design pa-

rameters such as Young's modulus, loading conditions and volume constraints, etc are treated deterministically in typical optimization problems, these properties and conditions must contain uncertainties and it is difficult to identify appropriate values in actual mechanical design problems. To overcome the effect of uncertainties, a conventional safety factor approach was adopted. However, this approach might overestimate or underestimate the effect of uncertainties. Furthermore, there exists a very active research field called "robust optimization" which treats these uncertainties theoretically. One significant approach is the "robust counterpart approach", which remodels the original problem including uncertainty into a new optimization problem having feasible solutions for the original problem. This idea was originated by Soyster [9] for the linear programming problem and early development was achieved by e.g. Falk [10] and Singh [11]. Important development of the approach is to be found in the work of Ben-Tal and Nemirovski [12, 13, 14], El Ghaoui and Lebret [15], El Ghaoui et al. [16] and Bertsimas and Sim [17] in the context of linear, conic, and quadratic programming. The detail of the "robust optimization" approaches considering uncertainties can be found in several comprehensive reviews (e.g. [18, 19, 20, 21] or Chapter 16-21 in [22]). These methods can provide appropriate robust optimal solutions that reasonably consider the uncertainties contained in actual design problems.

Recently, in the context of "Robust optimization", some topology optimization methodologies have been proposed. For example, Guest and Igusa performed continuum topology optimization under loading uncertainties based on multi-loading formulation composed of several load patterns including the probability function. The methodology has also been extended

to optimization under the uncertainties of nodal location in truss structures [23]. Luo et al., performed optimization under a non-probabilistic reliability constraint based on the convex model [24]. They applied this methodology to optimization which considers geometrical non-linearities [25] and extended the combination model with the probabilistic model [26]. In addition to structural stiffness optimization, the robust compliant mechanism design methodology under loading uncertainty was also proposed [27].

From this extensive field of research, in this paper we explore the stiffness maximization problem of structures considering uncertainties in the loading conditions (e.g. [23, 27, 28, 29, 30, 31, 32, 33, 34, 35]). As a part of the robust design for uncertain loads, the stiffness maximization under the worst load case in a set of prescribed uncertain loads is investigated. When the uncertainty property is prescribed as a convex set, the problem can be solved by the so-called convex model method [36]. In the convex model method, the uncertain parameters are bounded in a convex set such as a hypersphere, hyperellipsoid or hypercube without assuming a probabilistic distribution. The worst case is then identified by searching only within the bound of the convex set, when the criteria are evaluated as a convex function. However, to perform the optimization based on this concept, a nested optimization loop is usually performed to find the worst load case in addition to the ordinary outer optimization loop which updates the design variables.

On the other hand, a methodology that establishes the worst load case analytically without inner optimization has been proposed [29, 31, 32] based on the concept of "robust compliance", which is the work exerted by the uncertain load. The robust compliance minimization problem can be formu-

lated as the eigenvalue problem on the domain with respect to the uncertain loads and displacements [29, 31, 32].

In this study, the linear elastic structural problem is first considered as a linear operator of the force function on the displacement function before solving the eigenvalue problem directly. The value of the compliance can be analyzed using a spectrum method for the linear operator representing the structural characteristics under the constraint of the norm of the input force function, although the force function has uncertainty in robust optimization. Moreover, when the loading domain is limited in a small sub-domain of the linear elastic domain, it is reasonable to consider the loading sub-domain, not the full domain to calculate the robust compliance.

In this case, the large linear system of the full domain can be reformulated into a small linear system of a sub-domain to evaluate the uncertainty of loads in the limited small loading domain. A small size linear system consisting of the small loading domain is obtained from the full size linear system by the "aggregation" approach. The aggregation approach is used in the field of control for reducing the dimensions of large control systems or state equations to extract the required element from the large systems for incomplete state feedback control (see e.g. [37, 38]). This idea is useful in optimization. Aggregation enables us to formulate the minimum required simple linear system for optimization to evaluate the relationship of target elements of the system even if the original problem is very large. In our previous work, minimization of the detection error of robotics load cells was performed based on this concept [39].

In this paper, an effective formulation for the topology optimization prob-

lem is proposed, which is the stiffness maximization problem for the worst load case. An objective function is first set as the robust compliance for a linear elastic body. Then, the linear elasticity problem is discretized using the finite element method. An aggregated linear system composed of the local uncertain load vector and the local displacement vector defined for the loading sub-domain and a symmetric matrix connecting them, is constructed based on the discretized linear elasticity system. According to the Rayleigh-Ritz theorem for symmetric matrices, the robust compliance minimization problem is formulated as the minimization problem of the maximum eigenvalue of the matrix. The worst load case is easily established as the eigenvector corresponding to the maximum eigenvalue of the matrix. Particularly for point load problems, the eigenvalue represents the worst loading direction for the structure at the specified point.

The proposed structural optimization method is implemented using the topology optimization which achieves the most fundamental optimization of structures including changes in these topologies (number of holes). The update of the density function of the topology optimization is performed based on sensitivity analysis and the method of moving asymptotes (MMA) [40], which is an optimizer having numerous benefits in various optimization problems by virtue of its combination with topology optimization (see e.g. [6] and references therein). The numerical examples are provided to illustrate mechanically reasonable structures and establish the worst load cases corresponding to these optimal structures.

2. Formulation

2.1. Derivation of the aggregated system based on the finite element method

In this research, the stiffness maximization problem of linear elastic bodies when applying uncertain body forces, is considered. Let Ω, which is made of a homogenized isotropic material, be the domain that varies during the optimization process. The discretized linear elasticity problem using the finite element method is derived first since the proposed method can be applied to linear systems with finite dimensions:

$$\boldsymbol{K}\boldsymbol{U} = \boldsymbol{F} \tag{1}$$

where $\boldsymbol{K}$ is the stiffness matrix, $\boldsymbol{U}$ and $\boldsymbol{F}$ are the discretized displacement and force vectors.

For stiffness maximization problems under deterministic loads, the compliance, which is the work exerted by the load, is used as the objective function (see. e.g. [6]). As well as for the deterministic case, robust compliance is proposed for uncertain loads (where the load is treated as a function) [29, 31, 32]. Robust compliance can be formulated as follows using the discretized form,

$$c = \boldsymbol{F}^T\boldsymbol{U} \tag{2}$$

Compliance is a function of both the uncertain loads $\boldsymbol{F}$ and the displacement $\boldsymbol{U}$.

When the loading domain is a small sub-domain of the linear elastic domain, most of the elements of the load vector $\boldsymbol{F}$ are zero. Thus, the dimensions of robust compliance can be reduced as follows.

$$c = \boldsymbol{F}_l^T\boldsymbol{U}_l \tag{3}$$

where $\boldsymbol{F_l}$ is the local load vector composed of the non-zero elements of the global load vector $\boldsymbol{F}$. $\boldsymbol{U_l}$ is the local load vector corresponding to $\boldsymbol{F_l}$. The local force vector $\boldsymbol{F_l}$ and displacement vector $\boldsymbol{U_l}$ can be formulated as follows:

$$\boldsymbol{F} = \boldsymbol{H}\boldsymbol{F_l},\ \boldsymbol{F_l} = \boldsymbol{H}^T\boldsymbol{F} \tag{4}$$

$$\boldsymbol{U_l} = \boldsymbol{H}^T\boldsymbol{U} \tag{5}$$

where $\boldsymbol{H}$ is the matrix connecting the local and global vectors. The reason for retaining both $\boldsymbol{F} = \boldsymbol{H}\boldsymbol{F_l}$ and $\boldsymbol{F_l} = \boldsymbol{H}^T\boldsymbol{F}$ in Eq.(4) is that the elements of the vector $\boldsymbol{F}$ are all zero except for the elements corresponding to $\boldsymbol{F_l}$. Only Eq.(5) is defined with respect to the displacement vector $\boldsymbol{U}$. Using Eq.(1) and Eq.(4), $\boldsymbol{U_l}$ is also formulated as follows:

$$\begin{aligned} \boldsymbol{U_l} &= \boldsymbol{H}^T\boldsymbol{U} \\ &= \boldsymbol{H}^T\boldsymbol{K}^{-1}\boldsymbol{F} \\ &= \boldsymbol{H}^T\boldsymbol{K}^{-1}\boldsymbol{H}\boldsymbol{F_l} \\ &= \boldsymbol{C}\boldsymbol{F_l} \end{aligned} \tag{6}$$

where:

$$\boldsymbol{C} = \boldsymbol{H}^T\boldsymbol{K}^{-1}\boldsymbol{H} \tag{7}$$

$\boldsymbol{C}$ is an aggregated symmetric matrix with the same dimensions as the vectors $\boldsymbol{F_l}$ and $\boldsymbol{U_l}$. Eq.(6) is an aggregated system of the discretized equilibrium equation in Eq.(1), which directly shows the relationship between $\boldsymbol{F_l}$ and $\boldsymbol{U_l}$ used for calculating robust compliance in Eq.(3).

2.2. Formulation of the eigenvalue problem

Robust compliance in Eq.(3) can also be formulated using the local load vector $\boldsymbol{F_l}$ and the matrix $\boldsymbol{C}$ as follows:

$$c = \boldsymbol{F_l}^T \boldsymbol{C} \boldsymbol{F_l} \tag{8}$$

The constraint $||\boldsymbol{F_l}|| = 1$ is introduced for the uncertain local load vector $\boldsymbol{F_l}$, where $||\cdot||$ denotes the Euclidian norm. Under this constraint, the maximum and minimum of c are evaluated using the Rayleigh-Ritz theorem (see e.g. Chapter 4 in [41] or Chapter 2 in [42]) as follows:

$$\lambda_{\max}(\boldsymbol{C}) = \max \frac{\boldsymbol{F_l}^T \boldsymbol{C} \boldsymbol{F_l}}{\boldsymbol{F_l}^T \boldsymbol{F_l}} = \max_{||\boldsymbol{F_l}||=1} \boldsymbol{F_l}^T \boldsymbol{C} \boldsymbol{F_l} \tag{9}$$

$$\lambda_{\min}(\boldsymbol{C}) = \min \frac{\boldsymbol{F_l}^T \boldsymbol{C} \boldsymbol{F_l}}{\boldsymbol{F_l}^T \boldsymbol{F_l}} = \min_{||\boldsymbol{F_l}||=1} \boldsymbol{F_l}^T \boldsymbol{C} \boldsymbol{F_l} \tag{10}$$

where $\lambda_{\max}(\boldsymbol{C})$ and $\lambda_{\min}(\boldsymbol{C})$ are the maximum and minimum eigenvalues of $\boldsymbol{C}$. More specifically, the maximum robust compliance c is equal to the largest eigenvalue of the matrix $\boldsymbol{C}$ under the condition $||\boldsymbol{F_l}|| = 1$. Thus, minimization of the robust compliance will be achieved by minimizing $\lambda_{\max}(\boldsymbol{C})$. The following minimization problem of the maximum eigenvalue of $\boldsymbol{C}$ is equal to the minimization problem of the robust compliance in Eq.(3).

$$\underset{\Omega}{\text{minimize}}\, \lambda_{\max}(\boldsymbol{C}) \tag{11}$$

The condition $||\boldsymbol{F_l}|| = 1$ is introduced by pure mathematical reason to use the Rayleigh-Ritz theorem for robust compliance. However, in compliance minimization, the optimal results do not depend on the norm of the force. Thus, this constraint can be extended to the general case other than nominal norm load cases. On the other hand, the load uncertainty is usually defined

as a variation from the nominal load condition in the robust optimization problem. For example, the variation is modeled as a bounded convex set around the nominal value in the convex model. On the other hand, variation of the load uncertainty for robust compliance is defined as the bounded set with a fixed norm. The uncertainty set is modeled as a hypersphere center on the origin, which is considered a special case of the convex model with zero nominal value.

Note that the finite element method is used for the derivation of the aggregated linear system in Eq.(6) and the optimization problem in Eq.(11) above. Thus, the proposed theory is fundamentally based on the finite element method and the validity of the proposed theory is still unclear in terms of functional analysis for the continuum linear elasticity problem. However, since the computational analysis of the linear elasticity problem is usually performed by the finite element method, the proposed method is applicable to most engineering applications.

2.3. Clarification of the worst load case

The worst case compliance optimization was defined as being achieved by minimizing the maximum eigenvalue of the matrix $\boldsymbol{C}$. In the above optimization methodology, the worst load case can be established clearly based on the eigenvector $\phi_{\max}$ corresponding to the maximum eigenvalue $\lambda_{\max}$. Letting the worst load case satisfying Eq.(9) be $\boldsymbol{F_l}_{\text{worst}}$ and multiplying the left side of Eq.(9) by ${\boldsymbol{F_l}_{\text{worst}}}^T \boldsymbol{F_l}_{\text{worst}} = ||\boldsymbol{F_l}_{\text{worst}}||^2 = 1$, the following equation is obtained:

$$\begin{aligned} {\boldsymbol{F_l}_{\text{worst}}}^T \boldsymbol{C} \boldsymbol{F_l}_{\text{worst}} &= \lambda_{\max}(\boldsymbol{C}) {\boldsymbol{F_l}_{\text{worst}}}^T \boldsymbol{F_l}_{\text{worst}} \\ &= {\boldsymbol{F_l}_{\text{worst}}}^T \lambda_{\max}(\boldsymbol{C}) \boldsymbol{F_l}_{\text{worst}} \end{aligned} \tag{12}$$

That is,

$$\boldsymbol{C}\boldsymbol{F}_{\boldsymbol{l}\mathrm{worst}} = \lambda_{\max}(\boldsymbol{C})\boldsymbol{F}_{\boldsymbol{l}\mathrm{worst}} \tag{13}$$

The above equation is an eigenvalue equation for the maximum eigenvalue and the corresponding eigenvector. Thus, the worst load case $\boldsymbol{F}_{\boldsymbol{l}\mathrm{worst}}$ can be established as the eigenvector corresponding to the maximum eigenvalue of matrix $\boldsymbol{C}$.

2.4. Topology optimization

Topology optimization is used as an optimizer of the linear elastic domain Ω since this method can perform the more fundamental optimizations over arbitrary domains including shape and topology, *viz.* and the number of holes. The fundamental concept is to introduce a fixed, extended design domain D that includes *a priori*, the optimal shape Ω and utilization of the following characteristic function :

$$\chi(\boldsymbol{x}) = \begin{cases} 1 & \text{if} \quad \boldsymbol{x} \in \Omega \\ 0 & \text{if} \quad \boldsymbol{x} \in D \setminus \Omega \end{cases} \tag{14}$$

Using this function, the original design problem of Ω is replaced by a material distribution problem incorporating an elasticity tensor, $\chi\boldsymbol{A}$, in the extended design domain D, where $\boldsymbol{A}$ is the elasticity tensor of the original material of Ω. Unfortunately, the optimization problem does not have any optimal solutions in $L^{\infty}(D; \{0, 1\})$[5]. A homogenization method is used to perform the relaxation of the solution space [5, 8]. In this way, the original material distribution optimization problem with respect to the characteristic function is replaced by the optimization problem of the "composite" composed of the original material and a very weak material imitating void with respect to a

density function. The density function represents the volume fraction of the original material and can be regarded as a weak limit of the characteristic function.

The relationship between the material properties of the composite and the density function must be defined in addressing the optimization problem. The most widely used method that sets a completely artificial material property [43, 44, 45], called the "solid isotropic material with penalization" (SIMP) method, is used in this research. In this method, the relationship between the material properties of the composite and the density function is set using the following simple equation with the penalized material density :

$$\boldsymbol{A}^* = \rho^p \boldsymbol{A} \ (0 \leq \rho \leq 1) \tag{15}$$

where $\boldsymbol{A}^*$ is the material property of the composite, ρ is the density function representing the volume fraction of the original material and p is a positive penalization parameter. This method has the advantage of controlling the non-linearity between the material property of the composite and the density function. This has the significant role of avoiding the "gray" domain which is hard to judge as either a material or a void.

Finally, adding a volume constraint and introducing the vector $\boldsymbol{\rho}$ of the discretized density function, the topology optimization problem of the discretized linear elastic domain composed of n finite elements for robust compliance is formulated as follows:

$$\underset{\boldsymbol{\rho}}{\text{minimize}}\, \lambda_{\max}(\boldsymbol{C}) \tag{16}$$

where

$$\boldsymbol{C} = \boldsymbol{H}^T \boldsymbol{K}^{-1} \boldsymbol{H} \tag{17}$$

$$\boldsymbol{F} = \boldsymbol{H} \boldsymbol{F_l} \tag{18}$$

$$||\boldsymbol{F_l}|| = 1 \tag{19}$$

$$0 \leq \rho_i \leq 1, \text{ for } i = 1, ..., n \tag{20}$$

$$Volume(\boldsymbol{\rho}) \leq V^U \tag{21}$$

where $Volume(\cdot)$ denotes the function calculating the volume of the domain, and V^U is the upper limit of the volume.

3. Numerical implementation

3.1. Computation of the matrix $\boldsymbol{C}$

Since the equation of the matrix $\boldsymbol{C}$, Eq.(7) contains the inverse matrix of the stiffness matrix and the computation has a high cost, this equation is reformulated by introducing the adjoint variable matrix $\boldsymbol{Z}$ as follows:

$$\begin{aligned} \boldsymbol{C} &= \boldsymbol{H}^T \boldsymbol{K}^{-1} \boldsymbol{H} \\ &= \boldsymbol{Z}^T \boldsymbol{H} \\ &= \boldsymbol{Z}^T \boldsymbol{K} \boldsymbol{Z} \end{aligned} \tag{22}$$

where:

$$\boldsymbol{K} \boldsymbol{Z} = \boldsymbol{H} \tag{23}$$

The computational cost for the adjoint variable matrix $\boldsymbol{Z}$ is reasonable, and is equal to the number of columns of the matrix $\boldsymbol{H}$ multiplied by the cost

for solving the ordinal equilibrium equation in Eq.(18). When the number of degrees of freedom of the loading domain is large, a number of linear systems must be solved to calculate $\boldsymbol{Z}$. In this case, an additional technique will be required to reduce the computational cost such as first performing the LU decomposition of $\boldsymbol{K}$ and repeating only forward and backward substitutions to solve these linear systems.

The effectiveness of the proposed formulation is confirmed by a numerical experiment. Let $\boldsymbol{K}$ be a 10299×10299 sparse symmetric matrix with the condition number 473548.15 and $\boldsymbol{H}$ be a 10299×99 matrix. This setting corresponds to the 2D distributed load example mentioned below. The matrix $\boldsymbol{C}$ is calculated using one of the following three methods: 1) Calculate Eqs.(22) and (23) by a direct method which is the first LU decomposition and repeat the forward and backward substitutions, 2) Calculate (22) and (23) by an iterative method which is the preconditioned conjugate gradient method, 3) Calculate Eq.(7) directly by forming $\boldsymbol{K}^{-1}$ with LU decomposition. Table 1 shows the computational times for each method. The direct method for Eqs.(22) and (23) has the shortest computational time. Even if the direct method is not available because of memory limitations, the solution can be obtained using the iterative method with a shorter computational time than the original formulation. The original formulation had the worst computational time and, moreover, required a significant amount of memory to handle $\boldsymbol{K}^{-1}$.

Table 1: Comparison of computational times for calculating the matrix $\boldsymbol{C}$

Calculation method	Algorithm	Time(s)
Direct method for Eqs.(22) and (23)	LU decomposition	1.40
Iterative method for Eqs.(22) and (23)	Preconditioned conjugate gradient method	38.89
Original formulation in Eq.(7)	LU decomposition	99.11

*The numerical experiment condition - CPU:Intel Core i7-980X Extreme Edition, Memory:24GB, OS:Windows7 Ultimate 64bit, Language and Compiler:Matlab 2009a.

3.2. Sensitivity analysis

To perform optimizations, the method of moving asymptotes (MMA) [40], which requires a first-order sensitivity analysis of the objective function with respect to the design variable ρ, is used. The sensitivity of the maximum eigenvalue of the matrix $\boldsymbol{C}$ with respect to the i-th design variable ρ_i can be calculated as follows: (see e.g. [46]).

$$\frac{\partial \lambda_{\max}(\boldsymbol{C})}{\partial \rho_i} = {\boldsymbol{\phi}_{\max}}^T \frac{\partial \boldsymbol{C}}{\partial \rho_i} \boldsymbol{\phi}_{\max} \tag{24}$$

where $\boldsymbol{\phi}$ denotes the normalized eigenvector.

When the above maximum eigenvalue is a repeated eigenvalue, it is not differentiable in the normal sense. In this case, directional derivatives can only be obtained by solving the following eigenvalue problem [46, 47].

$$\boldsymbol{M} = \frac{\partial \lambda_j(\boldsymbol{C})}{\partial \rho_i} \boldsymbol{a},\ \boldsymbol{M} \in \mathbb{R}^{s \times s},\ \boldsymbol{a} \in \mathbb{R}^s \tag{25}$$

where:

$$M_{ij} = {\boldsymbol{\phi}_i}^T \frac{\partial \boldsymbol{C}}{\partial \rho_i} \boldsymbol{\phi}_j,\ i, j = 1, ..., s \tag{26}$$

s is the number of the repeated eigenvalue, $\boldsymbol{M}$ is the $s \times s$ matrix whose components are represented as Eq.(26), $\boldsymbol{a}$ is the $s-$dimensional eigenvector representing the derivative directions.

The matrix $\boldsymbol{C}$ has a similar form to the compliance matrix $\boldsymbol{U}^T\boldsymbol{K}\boldsymbol{U}$. Thus, $\partial\boldsymbol{C}/\partial\rho_i$ is calculated simply using the matrix $\boldsymbol{Z}$ in a similar way (see e.g. [6]). First, the equilibrium equation in Eq.(1) is substituted into Eq.(22) using another adjoint variable matrix $\boldsymbol{L}$ as follows:

$$\boldsymbol{C} = \boldsymbol{Z}^T\boldsymbol{K}\boldsymbol{Z} - \boldsymbol{L}^T(\boldsymbol{K}\boldsymbol{Z} - \boldsymbol{H}) \tag{27}$$

Calculating $\partial\boldsymbol{C}/\partial\rho_i$ using the above formulation, the following equation can be obtained:

$$\frac{\partial\boldsymbol{C}}{\partial\rho_i} = \left(\boldsymbol{H}^T - \boldsymbol{L}^T\boldsymbol{K}\right)\frac{\partial\boldsymbol{Z}}{\partial\rho_i} - \boldsymbol{L}^T\frac{\partial\boldsymbol{K}}{\partial\rho_i}\boldsymbol{Z} \tag{28}$$

If $\boldsymbol{L}$ satisfies the following adjoint equation, the first term of the above equation vanishes:

$$\boldsymbol{K}\boldsymbol{L} = \boldsymbol{H} \tag{29}$$

Since this is the same equation as Eq.(23), $\boldsymbol{Z}$ can be used instead of $\boldsymbol{L}$. Finally, $\partial\boldsymbol{C}/\partial\rho_i$ is obtained as follows:

$$\frac{\partial\boldsymbol{C}}{\partial\rho_i} = -\boldsymbol{Z}^T\frac{\partial\boldsymbol{K}}{\partial\rho_i}\boldsymbol{Z} \tag{30}$$

3.3. Filtering method

The SIMP method is used in this research. In the 2D problem, the SIMP method can encounter a numerical instability known as a checkerboard pattern [48, 49]. One way to prevent this problem is to use a so-called filtering technique (see [50] and the references therein). In this research, filtering is

implemented based on the projection method [51]. This method sets the design variables in addition to the density function and "projects" the design variable onto the density function using a projection function. By adjusting the effective range and shape of the function, the checkerboard problem can be avoided. The above functions are calculated numerically by appropriate discretization. Although the discretized design variable function was set to the nodes of the finite element mesh in the original paper [51], the function is discretized at the center of the element mesh in this research. With this method, a new projected density function μ is established, and its value calculated at the i-th control point, is as follows :

$$\mu(\boldsymbol{x}_i) = \frac{\sum_{j \in S_i} \rho(\boldsymbol{x}_j) w_i(\boldsymbol{x}_j - \boldsymbol{x}_i)}{\sum_{j \in S_i} w_i(\boldsymbol{x}_j - \boldsymbol{x}_i)} \tag{31}$$

where:

$$S_i = \{j \mid \boldsymbol{x}_j \in \Omega_{p_i}\} \tag{32}$$

$$\Omega_{p_i}(\boldsymbol{x}_i) = \{\boldsymbol{x} \mid ||\boldsymbol{x} - \boldsymbol{x}_i|| \leq r_{\min},\ \boldsymbol{x} \in D\} \tag{33}$$

where $\boldsymbol{x}_i$ is the location of the center of the i-th element, Ω_{p_i} is the effective circular area of the projection function w_i set on the the center of the i-th element, S_i is the set of indices for the control points in Ω_{p_i}, $\rho(\boldsymbol{x}_j)$ is the value of the original density function at the center of the j-th element, and $r_{\min}$ is the radius of the effective area of the projection function. The function w_i is a linear weighting function defined as :

$$w(\boldsymbol{x}-\boldsymbol{x}_i)=\begin{cases}\dfrac{r_{\min}-||\boldsymbol{x}-\boldsymbol{x}_i||}{r_{\min}} & \text{if} \quad \boldsymbol{x}\in\Omega_{p_i}\\ 0 & \text{if} \quad \boldsymbol{x}\in D\setminus\Omega_{p_i}\end{cases} \tag{34}$$

3.4. Algorithm

Based on the above numerical implementation techniques, the optimization procedure is constructed as follows:

1. Set an initial shape.
2. Iterate the following procedure until convergence:
   (a) Calculate the matrix $\boldsymbol{C}$ by the finite element method.
   (b) Calculate the objective function, $\lambda_{\max}(\boldsymbol{C})$, and the total volume.
   (c) Calculate the sensitivities of the objective function and the total volume.
   (d) Based on the sensitivities, update the design variables using the method of moving asymptotes (MMA) [40].

The proposed methodology is a minimization of the maximum eigenvalue problem which contains an inherent discontinuity and is hard to solve using the ordinal gradient based algorithm. In other words, if the target eigenvalue remains a repeated eigenvalue during the optimization iterations, it will be difficult to converge it to an optimum using the proposed MMA based optimization algorithm, even if the directional sensitivity in Eq.(25) is used. Such types of problem are outside the capacity of the proposed algorithm. Some sub-gradient type algorithms were proposed for these types of problem (e.g. [47, 52]). Depending on the problems, these algorithms should be introduced instead of the proposed MMA based algorithm.

4. Numerical example

The following numerical examples are provided to confirm the validity of the proposed method. All examples assume a virtual material with a normalized Young modulus E of 1.0 and a Poisson ratio ν of 0.3. The parameter $r_{\min}$ for the projection method used in Eq.(33) is set to 1.5 times the mesh size. Quadrangular and hexahedral isoparametric elements are used for discretizations in 2D and 3D, respectively. All optimal configurations are plotted as the distribution of the filtered density function of the optimal results.

4.1. 2D point load examples

4.1.1. Cantilever examples

As a benchmark problem for the proposed method, robust compliance minimization of a cantilever is performed as illustrated in Fig.1. The design domain is a 2×1 rectangle with a fixed boundary condition on the left side. The applied point of an uncertain load is set at the center of the right side. The minimized objective function is formulated as the highest eigenvalue of matrix $\boldsymbol{C}$ in Eq.(7). The volume constraint is set to 40% of the total volume. The domain is discretized with a 100×50 rectangular mesh. The initial value of the density function is 0.4 in all areas of the domain. The penalization parameter p in Eq.(15) is set to 1 and 3.

Figure 1 is about here.

Figure 2 shows the optimal configurations obtained after 100 iterations with $p = 1$ and 3. The optimal configuration is very similar to the typical

optimal configuration of the deterministic cantilever example [6]. Figure 3 shows the convergence history of the largest and second largest eigenvalues of the matrix $\boldsymbol{C}$. Since the size of the matrix $\boldsymbol{C}$ is 2×2, these eigenvalues correspond to the second and first eigenvalues. Smooth convergence of these eigenvalues can be observed in both cases.

Figure 4 shows the plots of the set of local load vectors $\boldsymbol{F_l}$ constrained by $||\boldsymbol{F_l}|| = 1$ and the set of displacement vectors $\boldsymbol{U_l}$ corresponding to these load vectors in Eq.(6) for the initial and optimal configurations obtained with $p = 3$. Since both vectors $\boldsymbol{F_l}$ and $\boldsymbol{U_l}$ have only 2 dimensions, they can be plotted on the plane. The set of $\boldsymbol{F_l}$ is represented as a unit circle. The circle is deformed to an ellipsoid by matrix $\boldsymbol{C}$ and this represents the set of the displacement vector $\boldsymbol{U_l}$. The eigenvector of matrix $\boldsymbol{C}$ is also shown in Fig.4. The normal and dotted arrows represent the second and first eigenvectors. The direction of the long axis of the ellipsoid, which is equal to the direction of the second eigenvector, is vertical. This indicates the loads with the vertical direction, $(0, 1)$ and $(0, -1)$ are the worst load cases in this example. This is a reasonable result in terms of the structural mechanics since horizontal cantilevers are clearly weaker with a vertical load than with a horizontal load. Figure 5 shows the history of the angle of the eigenvector representing the worst load direction with $p = 1$ and 3. Since these results were identical, only one line is shown in this graph. During the iteration, the direction stayed at a constant value of $\pi/2$. This indicates that, as a result, stiffness optimization against the vertical load was performed during the optimization process.

Figures 2,3,4,5 are about here.

To confirm the initial dependency of the proposed optimization problem, the optimization is performed with different initial shapes as shown in Fig.6. Figure 7 shows the optimal configurations obtained after 100 iterations with $p = 1$ and after 1000 iterations with $p = 3$. In the case of $p = 1$, the same results were obtained with Fig.2. In the case of $p = 3$, the result obtained with initial shape A is slightly different from Fig.2. However, since a high value of the parameter p increases the initial dependency, the proposed optimization problem does not have strong initial dependency and non-convexity. Figure 8 shows the first 10 iteration histories of the angle of the worst load direction for each case with $p = 3$. Since the results with $p = 1$ are identical, they are omitted. The initial worst load direction of the initial configuration B is horizontal which is different from the other results. This shows that the proposed method does not have strong initial dependency even in the case where the worst load case directions are different in the initial and the optimal configurations.

Figures 6,7,8 are about here.

4.1.2. Reverse L shaped examples

In the above example, the proposed method optimized the stiffness of a structure for the unit load with the worst direction. To confirm the utility of this function, another example is performed. The second target of the 2-D point load example is a reverse L-shaped design problem as shown in Fig.9. The top of the structure is fixed and the load point is set to the center of the left side. This is also a typical benchmark example. However, the worst

load direction is unclear and different from the previous cantilever example. The volume constraint is set to 50% of the total volume. The domain is discretized with a 0.02×0.02 size rectangular mesh. The initial value of the density function is 0.5 in all areas of the domain. The penalization parameter p in Eq.(15) is set to 3.

Figure 9 is about here.

Figure 10 shows the optimal configuration obtained after 100 iterations. Figure 11 shows the convergence history of the largest (the second) and second largest (the first) eigenvalues of the matrix $\boldsymbol{C}$. Figure 12 shows the plots of the set of local load vectors $\boldsymbol{F_l}$ satisfying $||\boldsymbol{F_l}|| = 1$ and the set of displacement vectors $\boldsymbol{U_l}$ corresponding to these load vectors in Eq.(6) for the initial and optimal configurations. Figure 13 shows the history of the angle of the second eigenvector. As shown in Fig.13, the worst load direction shows slight differences between the initial configuration and the optimal configuration and changed during the optimization process. The direction was tracked by the proposed method during the optimization procedure.

Figures 10,11,12,13 are about here.

The results were confirmed by solving the same optimization problem using the conventional optimization method and the inner optimization problem for establishing the worst load case. The optimization problem is formu-

lated as follows :

$$\underset{\boldsymbol{\rho}}{\text{minimize}} \underset{\boldsymbol{F_l},\ ||\boldsymbol{F_l}||=1}{\text{maximize}} \boldsymbol{F}^T\boldsymbol{U} \tag{35}$$

Since a point unit load is assumed in this example, the nested optimization problem can be solved by an optimization problem with a single design variable which is the loading angle. The problem is solved using the golden section search. The outer problem is the ordinary compliance minimization problem for the worst load case of each iteration. Figure 14 shows the optimization after 100 iterations. Since this result is quite similar to the one obtained by the proposed method, its validity was confirmed.

Figure 14 is about here.

The result is also compared with those obtained by minimizing the ordinal deterministic compliance under the horizontal and vertical loads at the load point. Figure 15 shows optimal configurations for these load cases. Except for the objective function, all optimization conditions were the same as in this example. The worst load directions of these optimal configurations were established by calculating eigenvectors of the matrix $\boldsymbol{C}$. The worst load directions of Fig.15(a) and (b) are $(-0.0982, -0.9952)^T$ and $(0.8223, -0.5690)^T$. Figure 15(a) certainly shows a weak stiffness for the vertical loads. To confirm the robustness of these structures, each of the optimal configurations shown in Fig.10 and Fig.15 was applied to its own the worst load and the most undeformable load case, and each compliance was calculated. The most undeformable load cases can be calculated as the first eigenvector of the matrix $\boldsymbol{C}$. Table 2 shows the comparison of these results. The optimal

configuration obtained by the proposed method had the highest performance for the worst load case. Moreover, it also achieved the lowest ratio between the compliance for the worst load case and the most undeformable load case, which is an important index of robustness.

Figure 15 is about here.

Table 2: Compliances of optimal configurations for the worst load cases and the most undeformable load cases

Optimal configuration in	Fig.10	Fig.15(a)	Fig.15 (b)
For the worst load case	95.7652	342.8997	123.4389
For the most undeformable load case	74.7486	24.4768	63.9296
Ratio of these compliances	1.2812	14.0092	1.9309

4.2. 2D distributed load examples

The proposed method was applied to a bridge-like structure under an uncertain vertical distributed load as shown in Fig.16. The bottom vertexes of the structure were fixed and the uncertain vertical distributed load was applied to the bottom. The domain was discretized with a 100×50 rectangular mesh. Since the load applied to the domain contained 99 nodes and only vertical forces were considered, $\boldsymbol{C}$ became a 99×99 symmetric matrix. The volume constraint was set to 50% of the total volume. The initial value of the density function was 0.5 in all areas of the domain. The penalization parameter p in Eq.(15) was set to 3.

Figure 16 is about here.

Figure 17 shows the optimal configuration obtained after 50 iterations. In this result, a structure similar to the actual bridge was obtained. Figure 18 shows the convergence history of the largest and second largest eigenvalues of the matrix $\boldsymbol{C}$. Smooth convergence can also be observed in the distributed load example as well as the previous point load examples, while the scale of the eigenvalue problem was much larger. Figure 19 shows the worst load distributions for the initial shape and the optimal configuration. These figures show that the worst load case has varied during the optimization process.

Figures 17,18,19 are about here.

The same optimization was performed with a different mesh discretization to confirm the mesh dependency of the proposed method. Due to the constraint $||\boldsymbol{F_l}|| = 1$, the shape of the load distribution can depend on the number of degrees of freedom considered in the loading domain. The domain was discretized with a coarser 50×25 rectangular mesh than the previous example. $\boldsymbol{C}$ became a 49×49 symmetric matrix. Figure 20 shows the optimal configuration obtained after 50 iterations and the corresponding worst load distribution. Although the values of the worst loads at each node on the loading boundary were higher than those of the previous example, the outline of the worst load distribution and the optimal configuration were quite similar to it.

Figure 20 is about here.

The optimal configuration in Fig.17 was compared with the optimal configurations obtained by the deterministic approach. Figure 21 shows the optimal configurations obtained by minimizing the ordinary deterministic compliance for a vertical point load at the bottom center, and for a uniform vertical distributed load on the bottom side, under the same optimization conditions as for this example. The worst load distributions of these configurations are also shown in Fig.22. Each of the optimal configurations shown in Fig.17 and Fig.21 was applied to its own worst load distribution shown in Fig.19(b) and Fig.22, and each compliance was calculated. Table 3 shows the comparison of these results. The optimal configuration obtained using the proposed method achieved the highest performance for each worst load distribution.

Figures 21,22 are about here.

Table 3: Compliances of optimal configurations for the worst load cases

Optimal configuration in	Fig.17	Fig.21(a)	Fig.21(b)
Compliance	0.3089	1.1350	0.3139

4.3. 3D example

The 3D point load problem illustrated in Fig.23 was investigated. The design domain was a $2.4 \times 1.2 \times 2.4$ rectangular solid with a fixed boundary

condition on the left side. The applied point of an uncertain load was set at the center of the right side. The minimized objective function was formulated as the highest eigenvalue of matrix $\boldsymbol{C}$ in Eq.(7). The volume constraint was set to 20% of the total volume. The domain was discretized with a $60\times30\times60$ cubic mesh. The initial value of the density function was 0.2 in all areas of the domain. The penalization parameter p in Eq.(15) was set to 3.

Figure 23 is about here.

Figure 24 and 25 shows a 0.5 iso-surface plot and the cross-sectional density distribution on the xz planes of the optimal configuration obtained after 50 iterations. Figure 26 shows the convergence history of the largest (the third), second largest (the second) and third largest (the first) eigenvalues of the matrix $\boldsymbol{C}$. Although two of the converged eigenvalues seem to have been switched in iteration 8, the maximum eigenvalue did not become a repeated eigenvalue and smooth optimization continued. Figure 27 shows a unit sphere representing the set of the unit local load vectors $\boldsymbol{F_l}$. Figure 27 (b) and (c) show the oval sphere representing the set of the displacement vector $\boldsymbol{U_l}$ corresponding to these load vectors in Eq.(6) for the initial configuration and optimal configurations. The three eigenvectors of matrix $\boldsymbol{C}$ are also shown in Fig.27. The third, the second and the first eigenvectors were $\boldsymbol{\phi} = (0,1,0)^T,\ (0,0,1)^T,\ (1,0,0)^T$ in the initial and optimal configurations. The initial and the optimal configurations had the same worst load directions. The cross section view of the oval sphere on the yz-plane was almost a circle in the optimal configuration which was different from the initial configuration.

This indicated the structure had the same stiffness for all unit point loads in the yz-plane at the loading point and high robustness for loads in the yz-plane. The robustness was also confirmed from a mechanical point of view. In Fig.24, the triangular overview yielded the stiffness in the z direction and two inside horizontal ribs yielded the stiffness in the y direction.

Figures 24,25,26,27 are about here.

As a final example, the 3D distributed load problem illustrated in Fig.28 was performed. The design domain was a $2.4 \times 1.2 \times 1.2$ rectangular solid. The bottom plane was set to the loading domain and the left and right edges of the bottom were supported. The minimized objective function was formulated as the highest eigenvalue of matrix $\boldsymbol{C}$ in Eq.(7). The volume constraint was set to 20% of the total volume. The domain was discretized with a $60 \times 30 \times 30$ cubic mesh. The initial value of the density function was 0.2 in all areas of the domain.

Figure 28 is about here.

Figure 29 shows the optimal configuration obtained after 50 iterations. A structure similar to the actual bridge was obtained for the 2D distributed load example. Figure 30 shows the convergence history of the largest and second largest eigenvalues of the matrix $\boldsymbol{C}$. Smooth convergence was observed without any eigenvalue switching or repeated eigenvalues. Figure 31 shows

the worst load distributions for the initial shape and the optimal configuration. The peak of the worst load distribution was observed on the center of the x direction as well as for the 2D example. The shape of the worst load distribution was varied during optimization due to the three ribs across the structure.

Figures 29,30,31 are about here.

5. Conclusions

An effective structural optimization methodology for a linear elasticity design problem subjected to an uncertain load is proposed in this paper. First, a linear elasticity problem was discretized by the finite element method. An aggregated linear system composed of the local uncertain load vector and the local displacement vector defined in the loading sub-domain, and a symmetric matrix connecting them, was constructed based on the discretized linear elasticity system. The robust compliance minimization problem was then formulated as the minimization problem of the maximum eigenvalue of the symmetric matrix, based on the Rayleigh-Ritz theorem for symmetric matrices. The worst load case was established as the eigenvector corresponding to the maximum eigenvalue of the matrix. This methodology was implemented as a topology optimization problem using the SIMP method, sensitivity analysis and the method of moving asymptotes (MMA). The numerical examples illustrated mechanically reasonable structures and the fact that the worst load case can be established. The eigenvector represents the direction of the

worst load at the specified point, particularly for the point load example, which can be a useful mechanical insight for an actual structural design.

This research is based on the idea of "aggregation" which is a traditional approach used for reducing the scale of target problems to construct systems for partially observed states. Representing the mechanical aspects of the structure as a simple linear system can be effective in structural optimization when optimizing the fundamental structural characteristic of an uncertain input. The worst load case for uncertain loads was evaluated in this research, while the measurement error of the robotic load cells for uncertain measured loads was evaluated in our previous research [39]. In future research, we hope to extend the methodology to other structural optimization problems of systems with uncertain inputs, such as in the design of compliant mechanisms and multi-physics actuators with uncertain inputs.

Acknowledgments

We would like to thank Prof. Makoto Ohsaki at Hiroshima University for his valuable comments and advice on robust optimization and sensitivity analysis for repeated eigenvalue problems. We are also deeply grateful to Prof. Krister Svanberg at Albanova University Center for providing the source code for the Method of Moving Asymptotes (MMA).

References

[1] W. S. Hemp, Optimum Structures, Clarendon Press, Oxford, 1973.

[2] O. Pironneau, Optimal Shape Design for Elliptic Systems, Springer-Verlag, New York, 1984.

[3] R. Haftka, Z. Gürdal, Elements of Structural Optimization, Kluwer Academic Publishers, Dordrecht, 1989.

[4] G. I. N. Rozvany, Structural Design via Optimality Criteria, Kluwer Academic Publishers, Dordrecht, 1989.

[5] G. Allaire, Shape Optimization by the Homogenization Method, Springer-Verlag, New York, 2001.

[6] M. P. Bendsøe, O. Sigmund, Topology Optimization: Theory, Methods, and Applications, Springer-Verlag, Berlin, 2003.

[7] J. Haslinger, R. A. E. Mäkinen, Introduction to Shape Optimization: Theory, Approximation, and Computation, SIAM, Philadelphia, 2003.

[8] M. P. Bendsøe, N. Kikuchi, Generating optimal topologies in structural design using a homogenization method, Comput. Meth. Appl. Mech. Eng. 71 (2) (1988) 197–224.

[9] A. Soyster, Convex programming with set-inclusive constraints and applications to inexact linear programming, Oper. Res. 21 (5) (1973) 1154–1157.

[10] J. Falk, Exact solutions of inexact linear programs, Oper. Res. 24 (4) (1976) 783–787.

[11] C. Singh, Convex programming with set-inclusive constraints and its applications to generalized linear and fractional programming, J. Optim. Theor. Appl. 38 (1) (1982) 33–42.

[12] A. Ben-Tal, A. Nemirovski, Robust convex optimization, Math. Oper. Res. 23 (4) (1998) 769–805.

[13] A. Ben-Tal, A. Nemirovski, Robust solutions of uncertain linear programs, Oper. Res. Lett. 25 (1) (1999) 1–14.

[14] A. Ben-Tal, A. Nemirovski, Robust solutions of linear programming problems contaminated with uncertain data, Math. Program. 88 (3) (2000) 411–424.

[15] L. El Ghaoui, H. Lebret, Robust solutions to least-squares problems with uncertain data, SIAM J. Matrix Anal. Appl. 18 (1997) 1035–1064.

[16] L. El Ghaoui, F. Oustry, H. Lebret, Robust solutions to uncertain semidefinite programs, SIAM J. OPTIM. 9 (1998) 33–52.

[17] D. Bertsimas, M. Sim, The price of robustness, Oper. Res. 52 (1) (2004) 35–53.

[18] A. Ben-Tal, A. Nemirovski, Robust optimization–methodology and applications, Math. Program. 92 (3) (2002) 453–480.

[19] G. Park, T. Lee, K. Lee, K. Hwang, Robust design: an overview, AIAA Journal 44 (1) (2006) 181–191.

[20] H. Beyer, B. Sendhoff, Robust optimization–a comprehensive survey, Comput. Meth. Appl. Mech. Eng. 196 (33-34) (2007) 3190–3218.

[21] G. Schuëller, H. Jensen, Computational methods in optimization considering uncertainties–an overview, Comput. Meth. Appl. Mech. Eng. 198 (1) (2008) 2–13.

[22] Y. Tsompanakis, N. D. Lagaros, M. Papadrakakis (Eds.), Structural Design Optimization Considering Uncertainties, Taylor & Francis, Leiden, 2008.

[23] J. Guest, T. Igusa, Structural optimization under uncertain loads and nodal locations, Comput. Meth. Appl. Mech. Eng. 198 (1) (2008) 116–124.

[24] Y. Luo, Z. Kang, Z. Luo, A. Li, Continuum topology optimization with non-probabilistic reliability constraints based on multi-ellipsoid convex model, Struct. Multidisc. Optim. 39 (3) (2009) 297–310.

[25] Z. Kang, Y. Luo, Non-probabilistic reliability-based topology optimization of geometrically nonlinear structures using convex models, Comput. Meth. Appl. Mech. Eng. 198 (41-44) (2009) 3228–3238.

[26] Z. Kang, Y. Luo, Reliability-based structural optimization with probability and convex set hybrid models, Struct. Multidisc. Optim. 42 (1) (2010) 89–102.

[27] N. Kogiso, W. Ahn, S. Nishiwaki, K. Izui, M. Yoshimura, Robust topology optimization for compliant mechanisms considering uncertainty of applied loads, J. Adv. Mech. Des. Syst. Manufac. 2 (1) (2008) 96–107.

[28] A. Ben-Tal, A. Nemirovski, Robust truss topology design via semidefinite programming, SIAM J. Optim. 7 (4) (1997) 991–1016.

[29] A. Cherkaev, E. Cherkaeva, Optimal design for uncertain loading condition. In Homogenization: In Memory of Serguei Kozlov, World Scientific, Singapore, 1999.

[30] M. B. Fuchs, E. Farhi, Shape of stiffest controlled structures under unknown loads, Comput. Struct. 79 (18) (2001) 1661–1670.

[31] E. Cherkaev, A. Cherkaev, Principal compliance and robust optimal design, J. Elasticity 72 (1) (2003) 71–98.

[32] E. Cherkaev, A. Cherkaev, Minimax optimization problem of structural design, Comput. Struct. 86 (13-14) (2008) 1426–1435.

[33] F. de Gournay, G. Allaire, F. Jouve, Shape and topology optimization of the robust compliance via the level set method, ESIAM COCV 14 (1) (2008) 43–70.

[34] S. Conti, H. Held, M. Pach, M. Rumpf, R. Schultz, Shape optimization under uncertainty - a stochastic programming perspective, SIAM J. Optim 19 (4) (2009) 1610–1632.

[35] H. Held, Shape Optimization under Uncertainty from a Stochastic Programming Point of View, Vieweg+Teubner, Wiesbaden, 2009.

[36] Y. Ben-Haim, I. Elishakoff, Convex Models of Uncertainty in Applied Mechanics, Elsevier, Amsterdam, 1990.

[37] M. Aoki, Control of large-scale dynamic systems by aggregation, IEEE trans. automat. contr. 13 (3) (1968) 246–253.

[38] N. Sandell Jr, P. Varaiya, M. Athans, M. Safonov, Survey of decentralized control methods for large scale systems, IEEE trans. automat. contr. 23 (2) (1978) 108–128.

[39] A. Takezawa, S. Nishiwaki, M. Kitamura, E. C. N. Silva, Topology optimization for designing strain-gauge load cells, Struct. Multidisc. Optim. 42 (3) (2010) 387–402.

[40] K. Svanberg, The method of moving asymptotes- a new method for structural optimization, Int. J. Numer. Meth. Eng. 24 (2) (1987) 359–373.

[41] R. A. Horn, C. R. Johnson, Matrix Analysis, Cambridge University Press, New York, 1985.

[42] G. Allaire, S. M. Kaber, Numerical Linear Algebra, Springer, New York, 2008.

[43] M. P. Bendsøe, Optimal shape design as a material distribution problem, Struct. Optim. 1 (4) (1989) 193–202.

[44] M. P. Bendsøe, O. Sigmund, Material interpolation schemes in topology optimization, Arch. Appl. Mech. 69 (9) (1999) 635–654.

[45] M. Zhou, G. I. N. Rozvany, The coc algorithm. ii: Topological, geometrical and generalized shape optimization, Comput. Meth. Appl. Mech. Eng. 89 (1-3) (1991) 309–336.

[46] E. J. Haug, K. K. Choi, V. Komkov, Design Sensitivity Analysis of Structural Systems, Academic Press, Orlando, FL, 1986.

[47] A. P. Seyranian, E. Lund, N. Olhoff, Multiple eigenvalues in structural optimization problems, Struct. Optim. 8 (4) (1994) 207–227.

[48] A. Diaz, O. Sigmund, Checkerboard patterns in layout optimization, Struct. Optim. 10 (1) (1995) 40–45.

[49] O. Sigmund, J. Petersson, Numerical instabilities in topology optimization: a survey on procedures dealing with checkerboards, mesh-dependencies and local minima, Struct. Optim. 16 (1) (1998) 68–75.

[50] O. Sigmund, Morphology-based black and white filters for topology optimization, Struct. Multidisc. Optim. 33 (4) (2007) 401–424.

[51] J. K. Guest, J. H. Prévost, T. Belytschko, Achieving minimum length scale in topology optimization using nodal design variables and projection functions, Int. J. Numer. Meth. Eng. 61 (2) (2004) 238–254.

[52] L. Krog, N. Olhoff, Optimum topology and reinforcement design of disk and plate structures with multiple stiffness and eigenfrequency objectives, Comput. Struct. 72 (4-5) (1999) 535–563.

List of figures

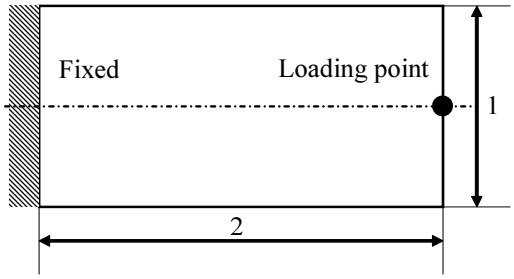

Figure 1: A cantilever design domain

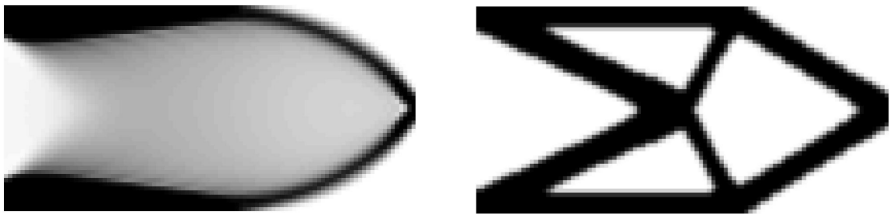

(a) $p = 1$ (b) $p = 3$

Figure 2: Optimal configurations of the cantilever example with $p = 1$ and 3

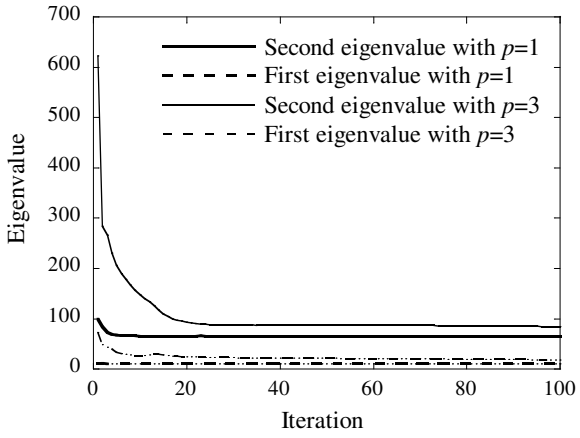

Figure 3: The convergence history of the eigenvalues of the cantilever example

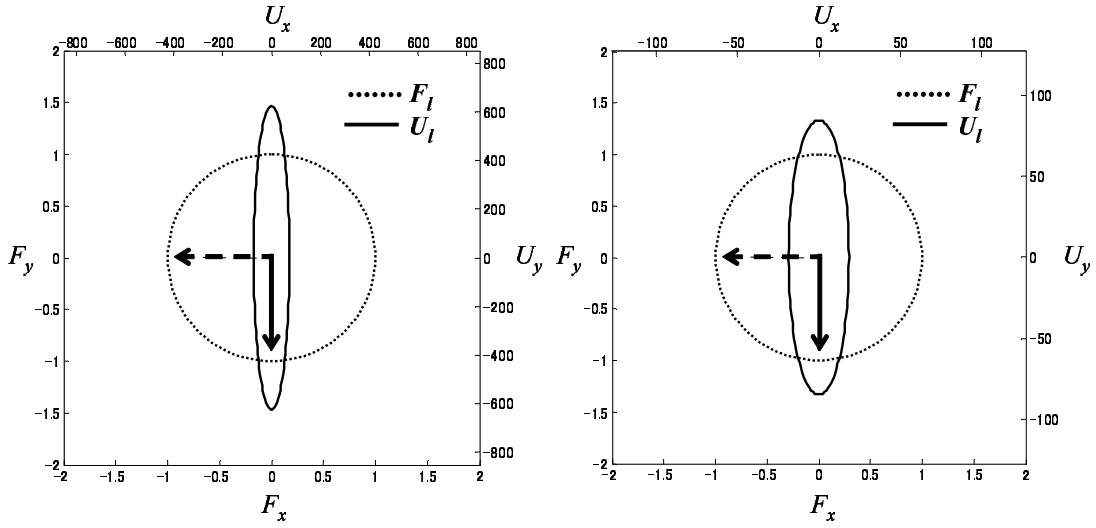

(a) Initial configuration (b) Optimal configuration

Figure 4: Illustrations of mapping from $\boldsymbol{F_l}$ to $\boldsymbol{U_l}$ using the matrix $\boldsymbol{C}$ in the cantilever example

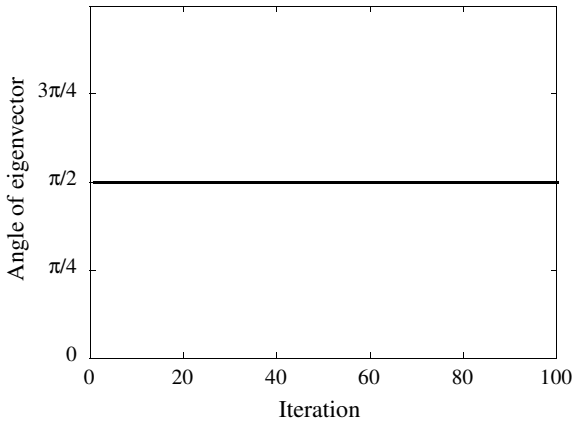

Figure 5: The history of the angle of the second eigenvector (the eigenvector corresponding to the worst load direction) of the cantilever example

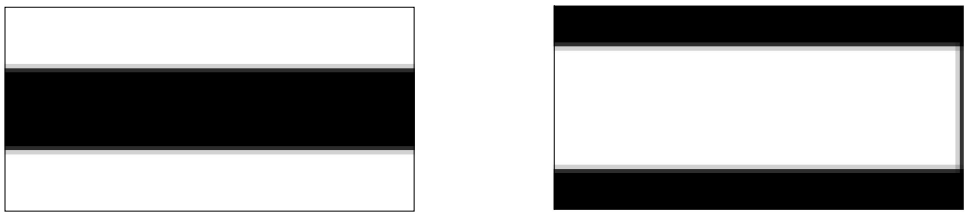

(a) Initial configuration A

(b) Initial configuration B

Figure 6: Initial configurations of the cantilever design domain

(a) With initial A and $p = 1$

(b) With initial A and $p = 3$

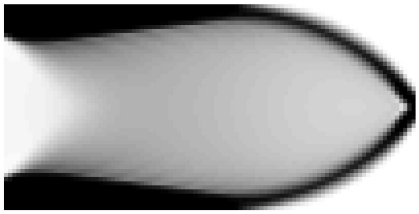

(c) With initial B and $p = 1$

(d) With initial B and $p = 3$

Figure 7: Optimal configurations with different initial configurations

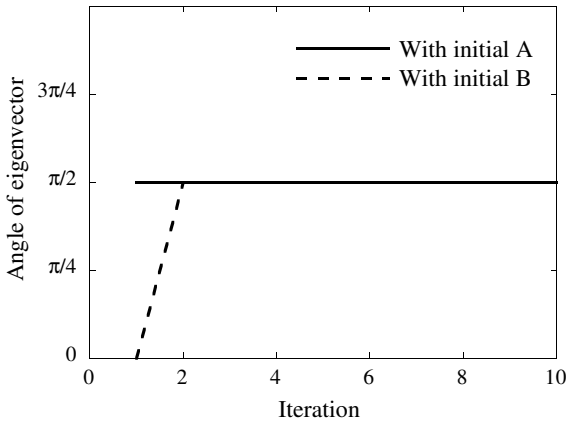

Figure 8: The history of the angles of the second eigenvectors with different initial configurations.

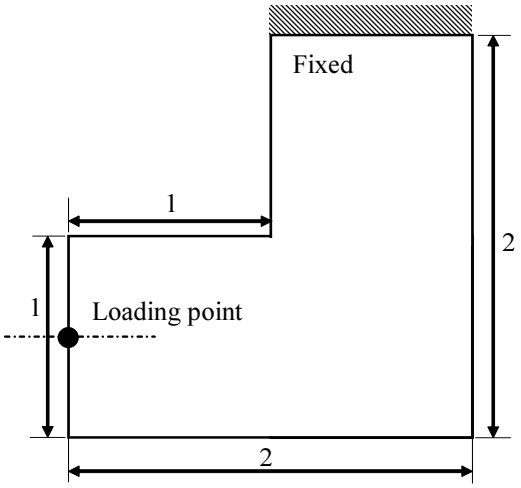

Figure 9: A reverse L shaped design domain

Figure 10: Optimal configurations of the reverse L example

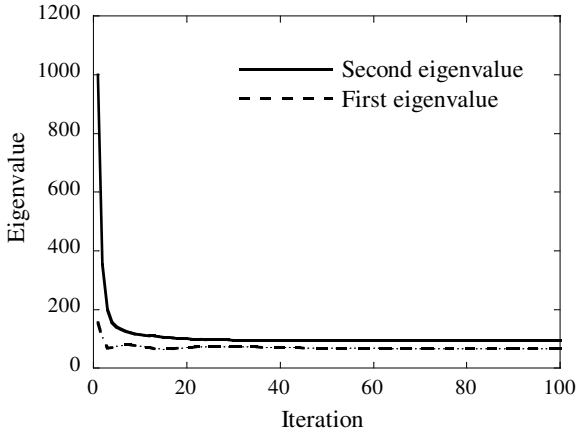

Figure 11: The convergence history of the eigenvalues of the reverse L example

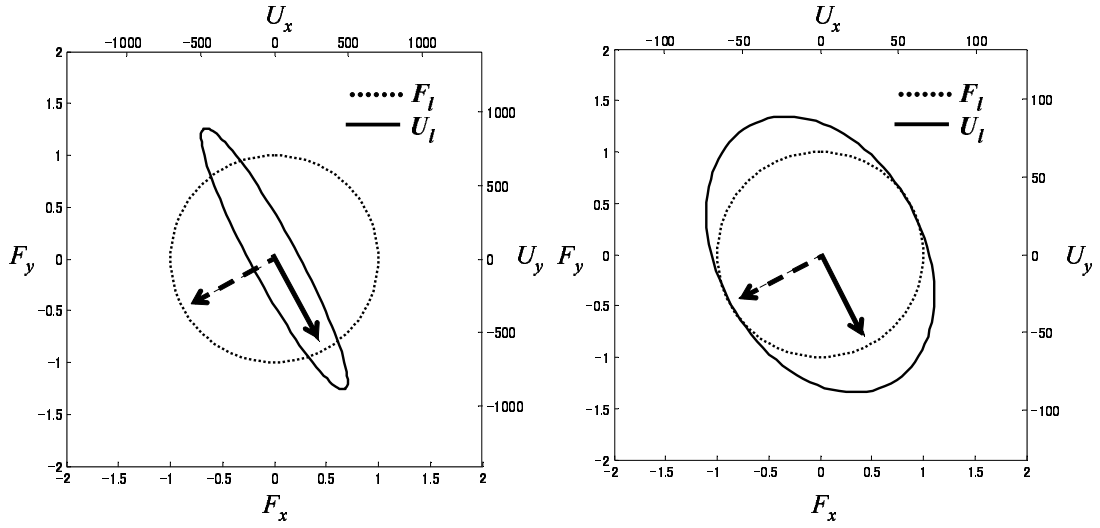

(a) Initial configuration (b) Optimal configuration

Figure 12: Illustrations of mapping from $\boldsymbol{F_l}$ to $\boldsymbol{U_l}$ using the matrix $\boldsymbol{C}$ in the reverse L example

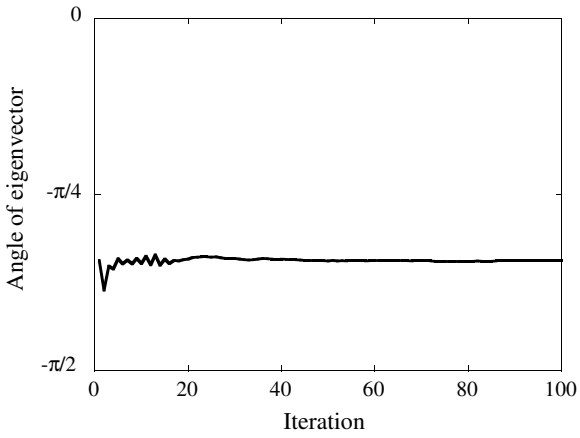

Figure 13: The history of the angle of the second eigenvector (the eigenvector corresponding to the worst load direction) of the reverse L example

Figure 14: Optimal configurations of the reverse L example obtained by solving the double loop optimization problem

(a) For horizontal load (b) For vertical load

Figure 15: Optimal configuration of the reverse L example obtained by the conventional deterministic approach.

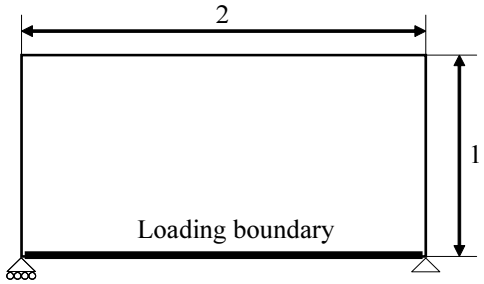

Figure 16: A bridge design domain

Figure 17: Optimal configurations of the bridge example

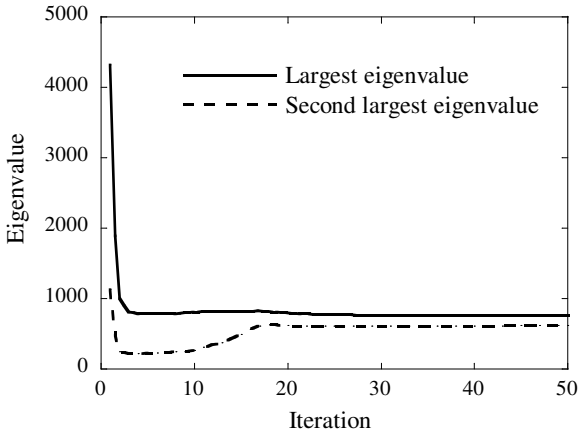

Figure 18: The convergence history of the eigenvalues of the bridge example

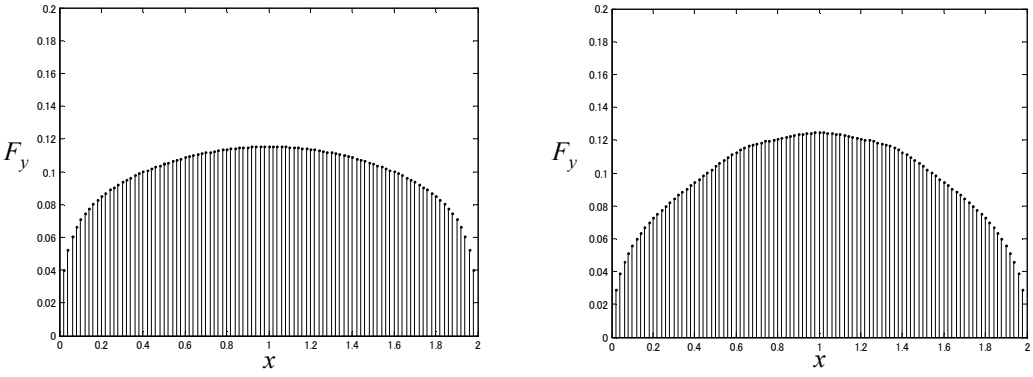

(a) Initial configuration (b) Optimal configuration

Figure 19: Illustrations of the worst load distributions of the bridge example

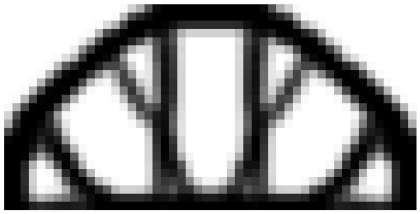

(a) Optimal configuration

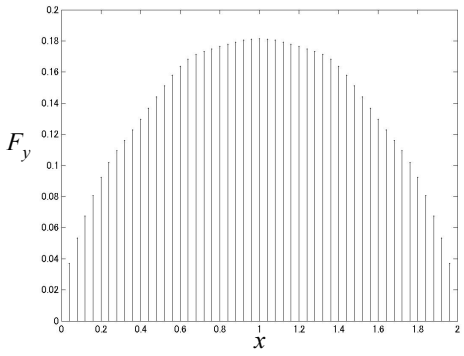

(b) The worst load distribution

Figure 20: Optimal configuration and the worst load distribution with a coarser mesh for the bridge example

(a) For a vertical point load at the bottom center

(b) For a vertical uniform distributed load on the bottom side

Figure 21: Optimal configurations of the bridge example obtained by the conventional deterministic approach

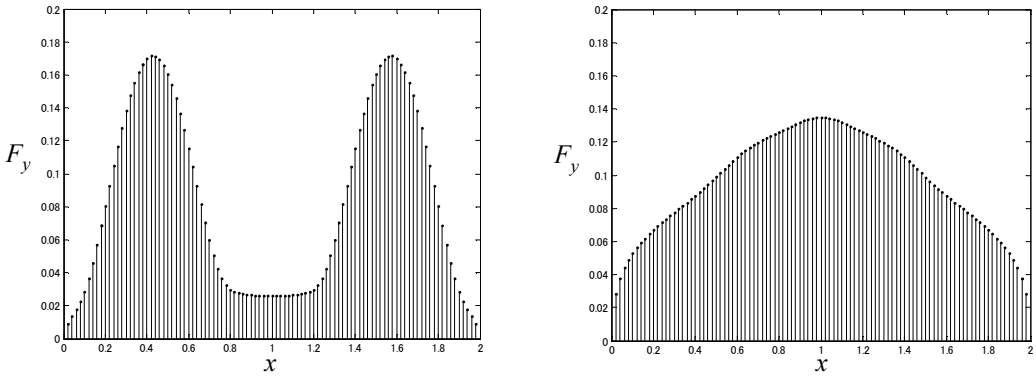

(a) The worst load distribution of Fig.21(a) (b) The worst load distribution of Fig.21(b)

Figure 22: The worst load distributions for optimal configurations obtained by the deterministic approach

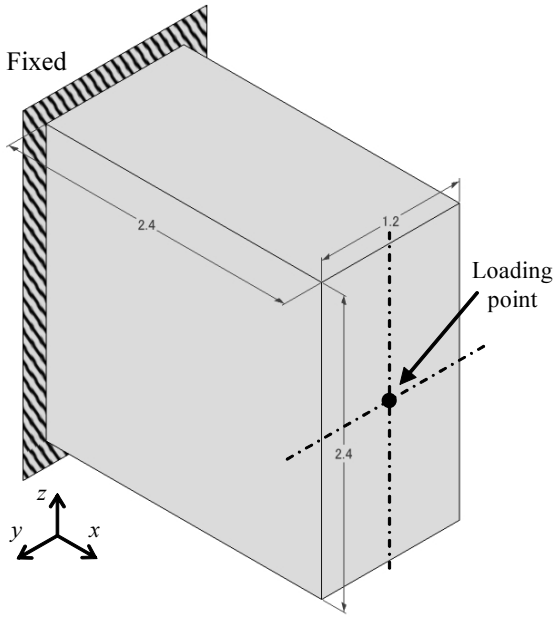

Figure 23: A 3D design domain

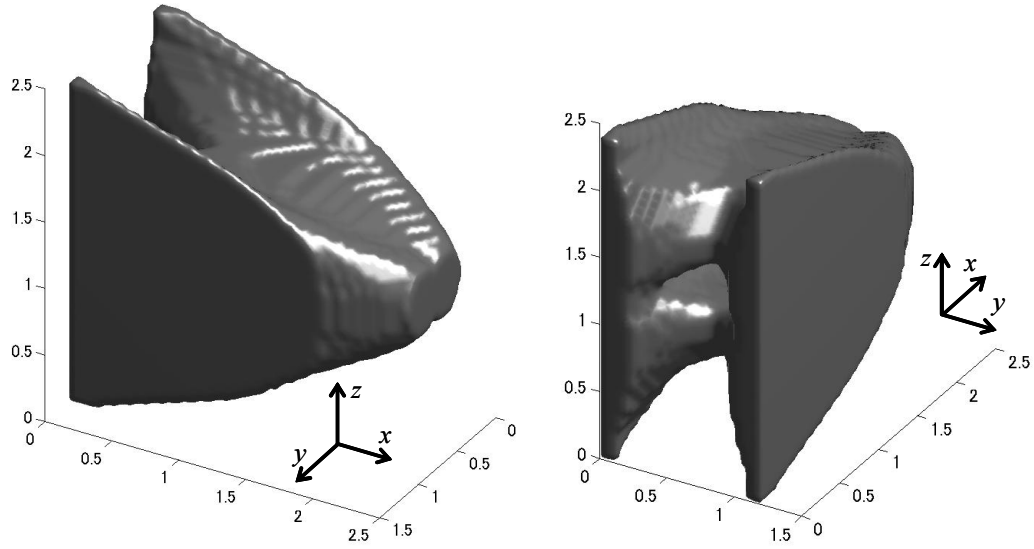

(a) Isometric view

(b) Isometric view from another viewpoint

Figure 24: Isosurface plots of the optimal configuration for the 3D example

(a) $y = 0$

(b) $y = 0.3$

(c) $y = 0.6$

Figure 25: Cross-section density distribution of optimal configurations of the 3D example on xz planes

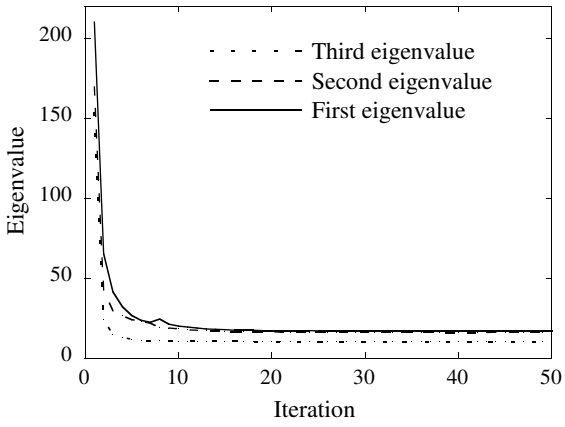

Figure 26: The convergence history of the eigenvalues of the 3D example

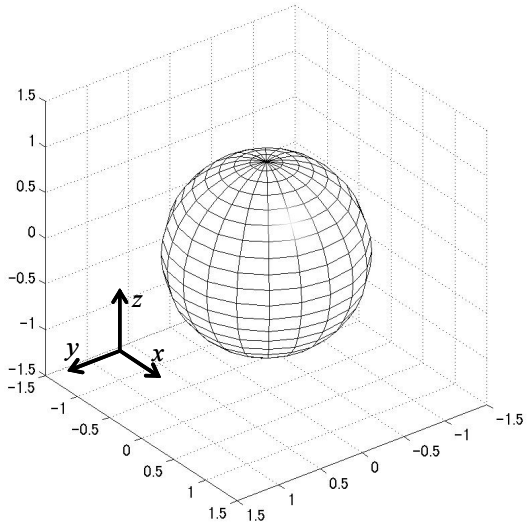

(a) Plot of the set of $\boldsymbol{F_l}$

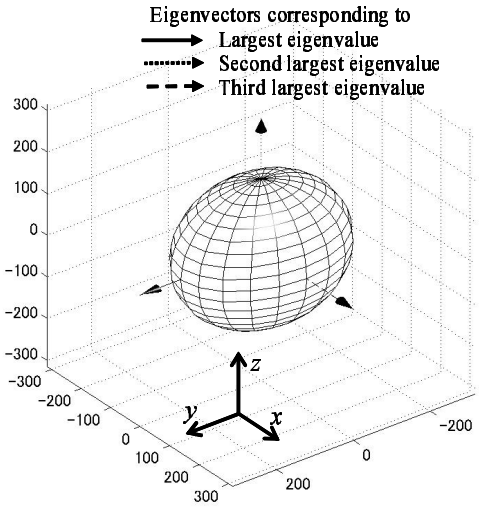

(b) Plot of the set of $\boldsymbol{U_l}$ of the initial configuration

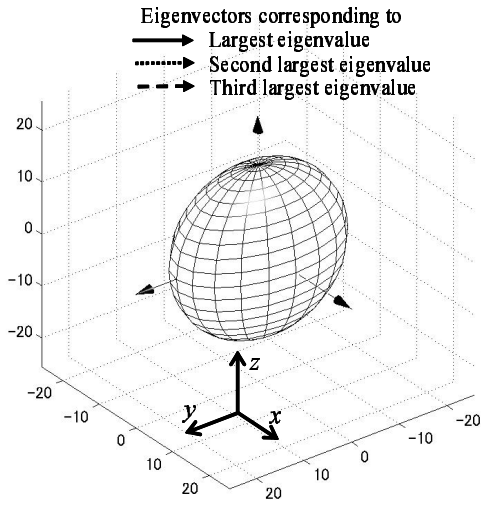

(c) Plot of the set of $\boldsymbol{U_l}$ of the optimal configuration

Figure 27: Illustration of mapping from $\boldsymbol{F_l}$ to $\boldsymbol{U_l}$ using the matrix $\boldsymbol{C}$ of the 3D example

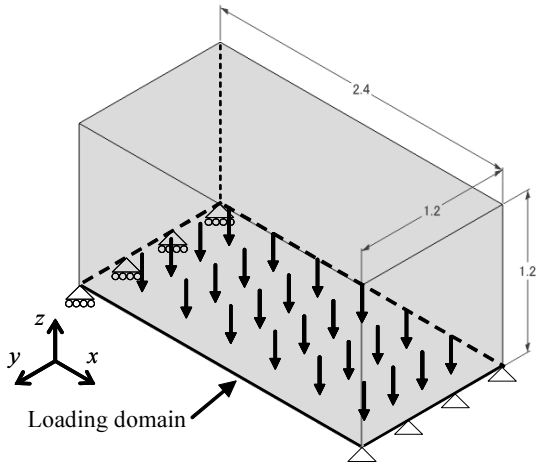

Figure 28: A 3D design domain under distributed load

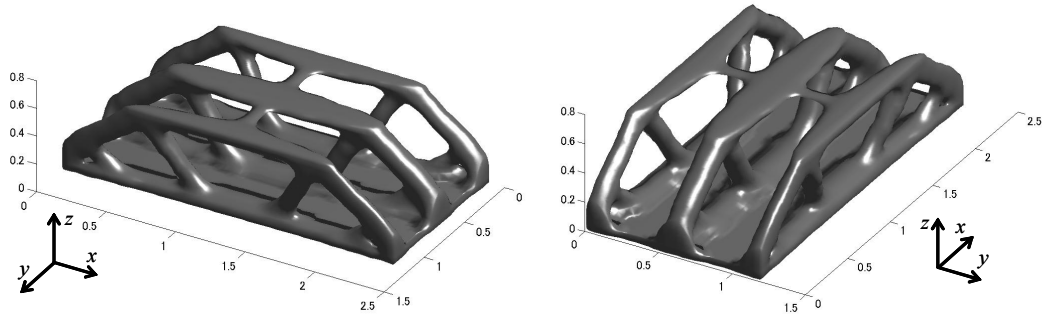

(a) Isometric view

(b) Isometric view from another viewpoint

Figure 29: Isosurface plots of the optimal configuration for the 3D distributed load example

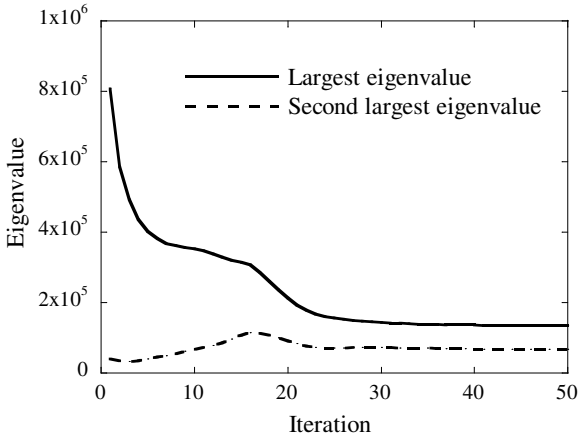

Figure 30: The convergence history of the eigenvalues of the 3D distributed load example

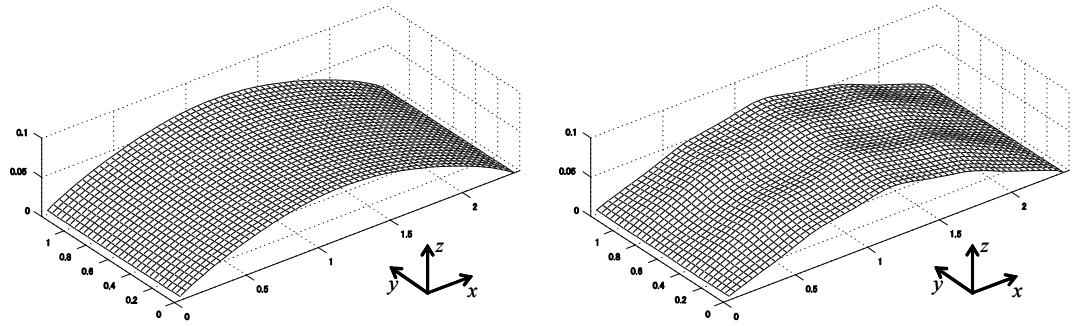

(a) Initial configuration (b) Optimal configuration

Figure 31: Illustrations of the worst load distributions of the 3D distributed load example